Available online at www.sciencedirect.com
SCIENCE DIRECT
ELSEVIER
Polymer 46 (2005) 10392–10404
polymer
www.elsevier.com/locate/polymer

Process and kinetics of order–order transition from bcc-sphere to hex-cylinder in polystyrene-*block*-polyisoprene-*block*-polystyrene: Time-resolved SAXS and TEM studies

Norihiro Sota, Takeji Hashimoto*

Department of Polymer Chemistry, Graduate School of Engineering, Kyoto University, Kyoto 615-8510, Japan

Received 27 June 2005; received in revised form 9 August 2005; accepted 13 August 2005
Available online 6 September 2005

Abstract

We have studied the process and kinetics of the order–order phase transition (OOT) from spheres in a body-centered-cubic lattice (bcc-sphere) to hexagonally packed cylindrical microdomains (hex-cylinder) for a polystyrene-*block*-polyisoprene-*block*-polystyrene triblock copolymer, induced by abrupt temperature drops. In this study, time-resolved small-angle X-ray scattering (SAXS) measurements are conducted to investigate the OOT processes *in situ* and at *real time*. Transmission electron microscopy observations for specimens rapidly frozen below the glass transition temperature at particular times in the OOT processes are also conducted to visualize the transient structures developed during the OOT. We elucidated the following pieces of evidence. (I) The OOT proceeds via the nucleation and growth process as follows: After quenching the specimen, the system stays at a bcc-sphere state in the incubation period, t_i. After this period, (II) anisotropic grains of hex-cylinder are nucleated at the vicinity of grain boundaries of bcc sphere. (III) The growth of the grains appears to be faster along the cylindrical axis than along the direction perpendicular to it, on the contrary to the growth of hex-cylinder from the disordered phase. The OOT involves deformation of spherical domains toward a [111] direction of a bcc lattice, followed by coalescence and connection of them to cylindrical microdomains. (IV) The rate of OOT as observed by time-resolved SAXS was found to depend on quench depth, ΔT ($\equiv T_{OOT} - T_{cyl}$) = 4–10 K, or thermodynamic driving force for the OOT, ε ($\equiv \Delta T/T_{OOT}$) = 0.0087–0.0217, where T_{OOT} is the OOT temperature between hex-cylinder and bcc-sphere: The larger ΔT or ε is, the shorter t_i is and the faster the transformation rate, R_T, is after the incubation time. (V) Consequently, the time change of a characteristic parameter as observed by SAXS at various ΔTs fall on to a master curve when real time is reduced with t_i, revealing that the following two intriguing conclusions: (i) t_i and R_T^{-1} have the same temperature dependence, and hence the system has only single time scale, and (ii) the transformation after the incubation period starts only when the characteristic parameter reaches a temperature independent critical value.

Keywords: Block copolymer; Order–order transition; Nucleation and growth

1. Introduction

Recently, block copolymers have been recognized as advanced nano-materials, because they could self-assemble into various patterns with nano-periodicity and can be used as templates for nano-fabrications toward advanced practical applications. A better control of the structures may require information on the process and kinetics of the phase transitions for the block copolymers, such as the order–disorder transition (ODT) and the order–order transition (OOT). In this work, we focus on kinetics and process of the thermally induced OOT from equilibrium bcc-sphere phase (spherical microdomains in body-centered cubic symmetry) to equilibrium hex-cylinder phase (cylindrical microdomains in hexagonal symmetry).

To our surprise, there are no reports on time-resolved small-angle X-ray scattering (SAXS) and small-angle neutron scattering studies about process and kinetics of the OOT from bcc-sphere to hex-cylinder, except for a very short report at a given quench depth, ΔT ($\equiv T_{OOT} - T_{cyl}$) = 11 K, by Kim and his coworkers [1], although the process

* Corresponding author. Tel.: +81 75 383 2619; fax: +81 75 383 2623.
E-mail address: hashimoto@alloy.polym.kyoto-u.ac.jp (T. Hashimoto).

0032-3861/$ - see front matter © 2005 Elsevier Ltd. All rights reserved.
doi:10.1016/j.polymer.2005.08.038

and mechanism have been actively studied by static methods [2–7] as will be detailed below. Here, T_{OOT} and T_{cyl} are, respectively, defined the OOT temperature and a measuring temperature below T_{OOT} where hex-cylinder exists at equilibrium. In this work, we aim to: (i) systematically study *in situ* and at *real time* kinetics of the OOT process as a function of ΔT by means of time-resolved SAXS; (ii) elucidate morphological changes with time during the OOT process. The latter study involves transmission electron microscopy (TEM) on the specimen quenched at particular times set during the OOT process, guided by time-changes in characteristic scattering parameters as analyzed from the time-resolved SAXS experiments.

The equilibrium phase behavior of block copolymers, especially AB-type diblock copolymers composed of A- and B-block chains, is well understood both theoretically [8,9] and experimentally [10,11]. In the weak segregation regime, the microdomain structure of the diblock copolymers depends not only on the volume fraction of constituent block chains, f, [12–14] but also on the product, χN, [8,12, 15–17] where χ is the Flory–Huggins segmental interaction parameter, and N is the total degree of polymerization, so that the diblock copolymers exhibit the OOT when χN is changed.

The thermally induced OOT was predicted by Leiber [15] for the first time about a quarter of a century ago. Since then, the theoretical studies were promoted further [16]. However, the OOT was not confirmed experimentally for some time after the Leibler's theoretical prediction. In 1993, Hashimoto and his coworkers experimentally found for the first time the thermoreversible OOT between hex-cylinder and bcc-sphere [3]. Since then, the studies about the OOT were advanced not only theoretically [8,9,18–25] but also experimentally. Especially, the OOT between hex-cylinder and bcc-sphere were most studied, [2,4–7,26–28] and as a consequence, the OOT process was elucidated as follows: In the OOT process from hex-cylinder to bcc-sphere, the cylinders are burst into a series of spheres with the cylindrical axes being transformed to the [111] direction of bcc-sphere as schematically shown in Fig. 1(a); On the other hand, in the OOT from bcc-sphere to hex-cylinder, spheres along the [111] direction of a bcc lattice are deformed and interconnected to cylinders, as also shown in Fig. 1(a) [4,7,26,28]. Here, Fig. 1(b) and (c) represent the illustrations of hex-cylinder viewed from the direction of cylindrical axes and bcc-sphere viewed from the [111] direction in a bcc lattice, respectively.

The reason why the OOT process and kinetics have been hardly explored *in situ* and at *real time* seems to be because the OOT, especially from hex-cylinder to bcc-sphere, occurs relatively fast, as estimated by calculation of the energy barrier between the two phases by Matsen [25]. This makes it difficult to follow the process *in situ* and at *real time*. By several theoretical approaches, kinetic pathways of the OOT have been evaluated, and the transient or

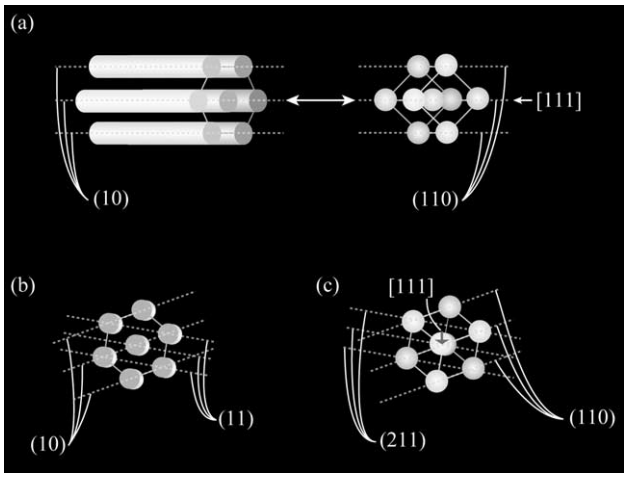

Fig. 1. (a) Schematic illustration showing the spatial arrangement of the microdomain structures before and after the OOT between hex-cylinder and bcc-sphere. The dotted lines indicate not only the directions of both cylindrical axes and the [111] direction in a bcc lattice but also the symmetry planes perpendicular to the plane of the paper. (b) Schematic illustration of hex-cylinder viewed from the direction of cylindrical axes. (c) Schematic illustration of bcc-sphere viewed from the [111] direction in a bcc lattice. Both in (b) and (c), the dotted lines represent the symmetry planes perpendicular to the plane of the paper.

metastable structures in the pathways have been presented [18–25]. However, unfortunately, they are not fully explored experimentally yet. In 1997, Sakamoto et al. reported the SAXS profiles and the linear dynamic mechanical response as a function of temperature for an asymmetric polystyrene-*block*-polyisoprene-*block*-polystyrene (SIS) triblock copolymer having its f lies near the borderline between hex-cylinder and bcc-sphere [2]. They elucidated that the OOT from hex-cylinder to bcc-sphere took place on heating process at ca. 183 °C for the SIS sample. Successively, in 1998, Kim et al. reported the OOT kinetics from bcc-sphere to hex-cylinder in the same triblock copolymer as Sakamoto et al. employed by using synchrotron small-angle X-ray scattering (SAXS) [1]. They presented the time evolutions of SAXS intensity profile, $I(q)$, magnitude of the scattering vector (q) at the first-order peak, q_m, the peak intensity, $I_m = I(q = q_m)$, and the square of the half-width at half maximum, σ_q^2, in the OOT process for only a single quench depth of 11 K. Here, q is defined by $q = (4\pi/\lambda)\sin(\theta/2)$ with λ and θ being the wavelength of the incident X-ray and the scattering angle, respectively. We think that more systematic time-resolved investigations as a function of ΔT are needed for a better understanding of the OOT process and kinetics of the triblock copolymer.

Therefore, we conducted the time-resolved SAXS and TEM experiments as described earlier. The TEM observations will help us to visualize transient structures developed during the OOT. The reciprocal-space observation by SAXS and the real-space observation by TEM are complementary, and they reinforce themselves each other.

The process and kinetics of the reverse OOT are also interesting research topics and shall be discussed in the other paper [29].

2. Experimental method

In this study, the SIS triblock copolymer (Vector4111, Dexco Polymers Co.) is used. The characteristics of this sample are as follows: the weight-averaged molecular weight, M_w, is 1.4×10^5; the polydispersity index, M_w/M_n, where M_n is the number-averaged molecular weight, is 1.11, and the weight fraction of polystyrene (PS) is 0.183 [2,30,31]. The block copolymer was dissolved into toluene with a small amount of antioxidant (Irganox 1010, Ciba-Geigy Group) and cast into film specimens from a 10 wt% solution by evaporating the solvent slowly in a fume hood for 1 week. The phase transition temperature of the film specimen was precisely reassessed by the temperature change of I_m and Bragg spacing, $D=2\pi/q_m$, obtained from the static SAXS experiments in the cooling cycle from 200 to 178 °C with a temperature decrement of 2 °C. Note that the specimen was first annealed for 30 min and then measured for 30 min at each temperature. According to the experiments, the OOT from bcc-sphere to hex-cylinder starts at 190 °C and completes at 186 °C. Therefore, T_{OOT} of the specimen is assessed to be 188 °C. This T_{OOT} is slightly different from that described in the previous works [2,30,31] because the film specimen for this study are prepared newly and differ from those used previously. The lattice disordering/ordering transition (LDOT) [32,33] temperature, T_{LDOT}, was assessed to be 215 °C.

The OOT from bcc-sphere to hex-cylinder was induced by a T-drop method from 195 °C where bcc-sphere exists at equilibrium, to $T_{cyl}=178$, 180, 182, 184 °C where hex-cylinder exists at equilibrium. The quench depths, ΔT, are 10, 8, 6, 4 K, respectively, and the thermodynamic driving forces, ε, defined as $\Delta T/T_{OOT}$, are 0.0217, 0.0174, 0.0130, 0.0087, respectively. The time-resolved SAXS method was done as follows: Before T-drop, the film specimen stuck in the sample holder [34] was put in a heater block, which was set on the optical path of the incident X-ray beam, at 195 °C above the T_{OOT} for 4 h. During the annealing time, time-resolved SAXS experiment was conducted to investigate whether the specimen reached the equilibrium bcc-sphere state or not. The scattering profile, especially I_m and the peak position of the first and higher order peaks did not change at all after 4 h, which, we considered, was a signature of the specimen to reach the equilibrium state, After reaching the equilibrium state, the temperature of the heater block was rapidly changed into T_{cyl}. After the specimen reached T_{cyl}, the time-resolved SAXS experiment was started, and the starting time was set zero at that time. The specimen reached T_{cyl} in ca. 2 min after T-drop. The 2 min delay is much shorter than the incubation period as will be clarified later.

The SAXS apparatus [35–37] used consists of an 18-kW rotating-anode X-ray generator (SRAM18XH MAC Science Co. Ltd) with a graphite crystal monochromator to obtain Cu Kα beam (wavelength is 0.154 nm) and a vacuum chamber for both the incident-beam path and scattered beam path. Moreover, in this study, one-dimensional position sensitive proportional counter (PSPC) together with line focus optics is used as a detector. It is because the 2D SAXS patterns of the initial bcc-sphere state and those during the OOT process are in circular rings around the incident beam due to randomly oriented poly-grain structures throughout the OOT process. The SAXS profiles were measured with the generator power of 12 kW (40 kV and 300 mA) and with varying exposure time to incident X-ray beam in the range of 60∼3000 s and corrected for the absorption of X-ray by the sample, air scattering, slit-height and slit-width smearing [35,36], and background scattering arising from thermal diffuse scattering (TDS) [38], unless otherwise stated. The intensity level of TDS was assumed to be a constant over the q-range covered in this experiment and was determined from the slope of Iq^4 vs q^4 plot at the high-q region ($q>0.7$–1.1 nm^{-1}) [39]. The absolute SAXS intensity was obtained by using the nickel-foil method [40].

TEM observations of the transient structures during the OOT process were also conducted to explore precisely the OOT mechanism. For the preparation of TEM observations, the specimens at given times after onset of the OOT were rapidly quenched into ice-water (at 0 °C). The quenched specimens could be frozen instantly because the glass transition temperature, T_g, of the matrix PS phase (ca. 100 °C) in the block copolymer is higher than 0 °C. The frozen specimens were microtomed into the ultrathin sections of ca. 50 nm thickness using a Reichert Ultracut S with the cryochamber FCS operated at −100 °C and a diamond knife (DiATOME, Switzerland). The ultrathin sections, thus, obtained were picked up on 100 mesh copper grids covered with a supporting film, which is made of 1% chloroform solution of poly(vinyl formal), and stained by the vapor of 2% osmium tetraoxide (O_SO_4) (aq) for 1 h at room temperature to stain selectively polyisoprene (PI) domains [41,42]. Then the microdomain structures in the ultrathin sections were observed by a TEM (JEOL JEM-2000FXZ) operated at 120 kV.

3. Results and discussion

3.1. Time evolution of the SAXS

3.1.1. Overall trend

First, we shall report the OOT process induced by the shallowest quench, $\Delta T=4$ K, to discuss the detailed process and mechanism. Fig. 2 shows the time evolution of the SAXS profile after T-drop from 195 to 184 °C. Here, we deliberately show the profiles without the slit corrections

and without the TDS correction to prevent any artifacts that might be induced by the corrections. In the SAXS profile just after T-drop, higher-order peaks can be seen at $q = \sqrt{2}q_m$ and $\sqrt{3}q_m$. The SAXS profiles do not appear to change so much for ca. 1600 s after T-drop. After this period, the higher-order peak at $q = \sqrt{2}q_m$ starts to decrease its intensity and eventually disappears, and those at $q = \sqrt{3}q_m$ and $\sqrt{4}q_m$ are becoming higher and sharper with time. Finally, the higher-order peaks can be seen only at $q = \sqrt{3}q_m$ and $\sqrt{4}q_m$.

To follow up the change of the first-order peak, the time evolutions of I_m, σ_q^2, and D are presented in Fig. 3. The three characteristic parameters were obtained from the SAXS profiles corrected for the slit smearings. Points at which some of the parameters characteristically change are marked by A, B and C. Then the OOT process is divided into four periods, I, II, III and IV separated by these points. In period I, I_m and σ_q^2 are almost constant, but D is slightly increasing. In period II, I_m still hardly changes, while σ_q^2 and D increase dramatically. On the contrary, I_m increases and σ_q^2 decreases, while D still increases continuously in period III. At point B, I_m starts to increase, while σ_q^2 and D show a maximum and an inflection point, respectively. Finally, I_m and D increase but σ_q^2 decreases gradually in period IV. Note that point C is fixed as follows: D increases almost linearly with log(time) in period IV as indicated by a gray line in Fig. 3(c). Therefore, the time when D reaches a value on the gray line is defined as point C.

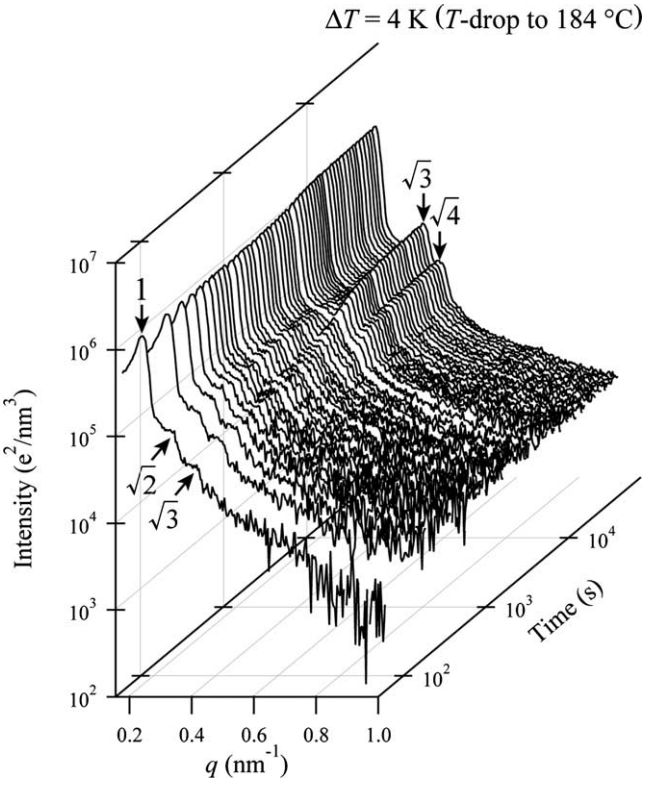

Fig. 2. Time evolution of the SAXS profiles for the SIS triblock copolymer after T-drop from 195 to 184 °C. The profiles without slit corrections are deliberately shown here to prevent any artifacts that might be induced by the slit corrections. q is a magnitude of scattering vector defined in the text.

3.1.2. Incubation period

Period I is an incubation period, which persists as long as about 1600 s, where bcc-sphere is kept as a metastable

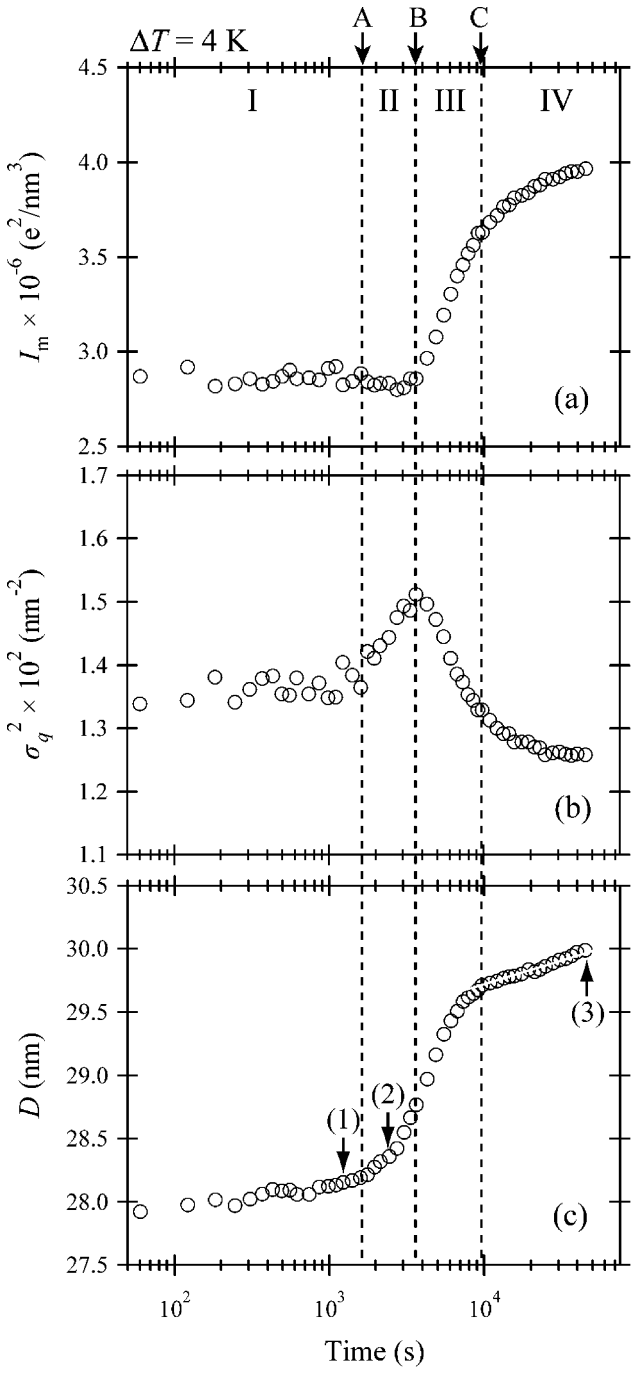

Fig. 3. Time evolutions of (a) the peak intensity, I_m, (b) the square of the half-width at half maximum, σ_q^2, (c) the Bragg spacing, D, obtained from the desmeared SAXS profile for the SIS triblock copolymer after T-drop from 195 to 184 °C. The time evolutions of the three variables are divided into four periods, I, II, III and IV separated by the three points, A, B, and C. The specimens are frozen for TEM observations at the time shown by the arrows numbered (1)–(3).

structure. This is obvious because the SAXS profiles hardly change, the higher-order peaks can be clearly seen at $q = \sqrt{2}q_m$ and $\sqrt{3}q_m$ in Fig. 2, and moreover I_m and σ_q^2 are almost constant. Nevertheless, D is slightly increasing. Since the system forms bcc-sphere, D indicates the Bragg spacing of (110) planes in a bcc lattice, D_{110}. When bcc-sphere is interconnected along the [111] direction and then transformed to hex-cylinder, it is necessary that D_{110} should be adjusted to D_{10}, as illustrated in Fig. 1(a). However, as found from Fig. 3(c), D_{110} is smaller than D_{10} by ca. 2 nm. Therefore, the slight increase of D in the incubation period may indicate a signature of pretransitional phenomenon. The increase of D is a natural consequence of the increased segregation power after the T-drop. The quench depth from T_{LDOT} was increased from 20 K for the equilibrium bcc-sphere phase at 195 °C to 31 K for the metastable bcc-sphere at 184 °C. D reaches a critical value of D_{110} at point A, beyond which bcc-sphere starts to be transformed into hex-cylinder. Existence of the incubation period suggests that this OOT proceeds via the nucleation and growth process and that the OOT is first-order phase transition.

Fig. 4(a) shows the scaled structure factors [43–45] obtained at various times during the incubation period. The universality of the structure factors with time suggests that the symmetry of bcc-sphere is maintained during period I, although the characteristic length, D, slightly increases. This means that bcc-sphere slightly expands both in terms of the cell unit and average radius of sphere, keeping the volume fraction identical. Note that a small bump at $q/q_m \cong 1.2$ is an error caused by desmearing of a sharp scattering profile.

3.1.3. OOT process

Bcc-sphere transforms into hex-cylinder in period II and III, where the SAXS profiles in Fig. 2 and the three parameters in Fig. 3 change dramatically. Now that this

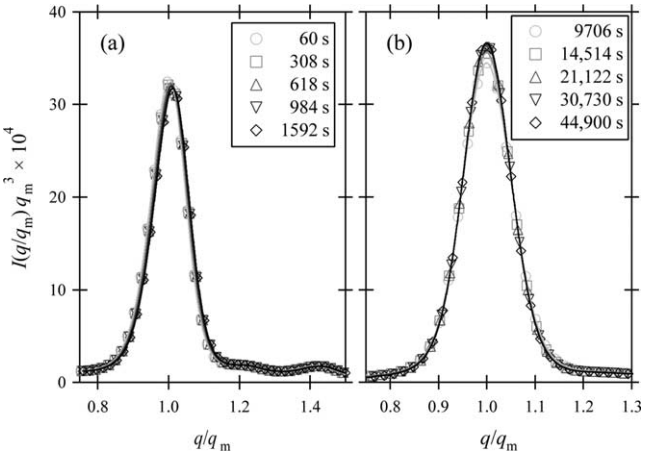

Fig. 4. Time evolutions of the scaled structure factor at various times: (a) metastable bcc-sphere phase in period I and (b) volume-filled hex-cylinder phase in period IV, shown by the plots of $I(q/q_m)q_m^3$ vs q/q_m. The scaled structure factors are shown to be universal with time.

OOT is found to proceed via the nucleation and growth process, the time-evolutions of I_m, σ_q^2, and D in those period should reflect coexistence of the bcc-sphere phase and the hex-cylinder phase. Fig. 5 highlights the time-evolution of the desmeared first-order peak (part a) and our interpretation of the results (part b). The illustration in Fig. 5(b) shows the way how the first-order peak changes with time in period II and III. At point A (1592 s), i.e. at the time just before the OOT starts, the system is occupied only by metastable bcc-sphere, so that the first-order peak is sharp (bright gray peak in Fig. 5(b)). When the OOT starts via the nucleation and growth process, grains of hex-cylinder are formed in the matrix of bcc-sphere and coexist with bcc-sphere in the system. Therefore, not only the scattering peak, which comes from the bcc-sphere phase but also that from the hex-cylinder phase (dark gray peak in Fig. 5(b)) contributes to the net scattering peak, with the relative contribution of them depending on volume fraction of each phase in the system. D_{10} is larger than D_{110} as mentioned above, so that the scattering peak from the hex-cylinder phase appears at smaller q than that from bcc-sphere. By taking into consideration that the scattering intensity which comes from the equilibrium hex-cylinder phase is stronger than that which comes from the metastable bcc-sphere phase, we can expect that I_m and σ_q^2 evaluated from the net scattering profile (shown by the broken line) exhibit the following change with time: I_m hardly changes but σ_q^2 increases to a maximum value until bcc-sphere and hex-cylinder occupy the whole sample space almost by half and half at point B (3648 s). The volume fraction of hex-cylinder exceeds that of bcc-sphere in period III. Hence, I_m increases but σ_q^2 decreases. Finally, the sharp scattering peak which comes only from the hex-cylinder phase is appeared at point C (9706 s). During the periods II and III, D evaluated from the net scattering profile should increase sigmoidally with time. Thus, the reason why the three parameters change as shown in Fig. 3 is well interpreted as a consequence that the OOT proceeds via the nucleation and growth process, reflecting the first-order phase transition.

In this paper, we shall not decompose the net first-order peak profile obtained during the OOT process into those from bcc-sphere and hex-cylinder. This is simply because the two peaks from the coexisting two phases locate so close each other that it is almost impossible for us to unequivocally decompose it into the two profiles. Instead, we shall analyze the characteristic parameters, I_m, σ_q^2 and D evaluated from the net scattering profile as a function of time and interpret them qualitatively in terms of time changes in a relative contribution of the two phases based on the model shown in Fig. 5(b).

3.1.4. Final stage

At point C, the OOT almost completes where almost all the sample space is expected to be occupied by hex-cylinder. We will give a discussion on the reason why the

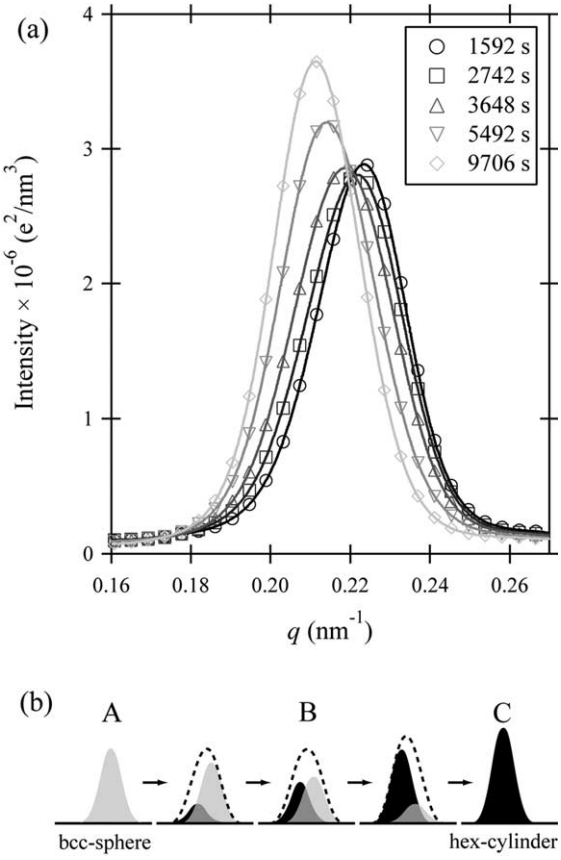

Fig. 5. (a) Time evolution of the first-order peak in the SAXS profiles after *T*-drop from 195 to 184 °C. (b) Schematic illustration showing the time-evolution in the first-order peak in the SAXS profiles. In the schematic illustration, the bright gray part, the dark gray part, and the black dotted line show the scattering which comes from bcc-sphere phase, the scattering which comes from hex-cylinder phase, and the net total scattering, respectively.

three variables in Fig. 3 change gradually in period IV together with the TEM results later.

Fig. 4(b) shows the scaled structure factors obtained at various times in period IV. Though the characteristic parameters change with time as shown in Fig. 3, we find that the scaled structures factors are almost universal with time. This means that during this period hex-cylinder expands in terms of both inter-cylinder distance and cylinder radius, keeping the volume fraction of cylinders constant. Therefore, the change of hex-cylinder occurs self-similarly with time. Needless to state that the universal scaled structure factor cannot be obtained in the transition period II and III, because microdomain structures change with time from bcc-sphere to hex-cylinder.

3.2. SAXS profiles measured before and after freezing

For the TEM observations of the specimens in the OOT process, the specimens were frozen with ice-water at particular times during the OOT at $\Delta T = 4$ K, which are indicated by arrows with the numbers in parentheses in Fig. 3. The SAXS profiles have been measured before and after freezing to check whether or not the freezing processes change the structure in the system. Fig. 6 shows the profiles measured before and after freezing at (a) 1228 s, (b) 2440 s and (c) 44,900 s after *T*-drop to 184 °C, each of which, respectively, corresponds to points (1)–(3) in Fig. 3. These profiles are not deliberately corrected for slit smearing to prevent any artifacts. As in the previous studies, [30,31] the freeze-in process in this study hardly changes the characteristics of the profiles at small q region ($q < 0.4\ \mathrm{nm}^{-1}$). Hence, the structure at a large length scale associated with spatial arrangement of spheres or cylinders are essentially unaltered during the freezing process. However, the processes affect the profiles at a large q region ($q > 0.4\ \mathrm{nm}^{-1}$) and hence local structures of the system as described below.

Point (1) in Fig. 3 is almost at an end of the incubation period, so that the system at this point forms metastable bcc-sphere as mentioned above. In Fig. 6(a), both profiles after and before freezing have higher-order peaks at $q = \sqrt{2}q_m$ and $\sqrt{3}q_m$, proving the structure at that point to be bcc-sphere. Moreover, a broad scattering maximum at $q = 0.57\ \mathrm{nm}^{-1}$ marked by a thick arrow can be seen in the profile after freezing but not in that before freezing. This maximum indicates that the particle scattering from spheres, namely the scattering from form factor, appears because the interface between PS spheres and PI matrix is sharpened by freezing, as reported in the previous studies [30,31]. Point (2) in Fig. 3 is the time just after the onset of the OOT. In Fig. 6(b), both profiles after and before freezing have higher-order peaks at $q = \sqrt{2}q_m$ and $\sqrt{3}q_m$ and a broad scattering maximum at $q = 0.57\ \mathrm{nm}^{-1}$ marked by a thick arrow, reflecting that bcc-sphere still dominates hex-cylinder. However, the higher-order peak at $q = \sqrt{3}q_m$ ($0.37\ \mathrm{nm}^{-1}$) in Fig. 6(b) is slightly shifted to smaller q than that ($0.40\ \mathrm{nm}^{-1}$) in Fig. 6(a). We shall prove later that this indicates the formation of hex-cylinder in the bcc-sphere phase. Point (3) in Fig. 3 is the time when hex-cylinder has already filled the whole sample space. In Fig. 5(c), both profiles after and before freezing have higher-order peaks at $q = \sqrt{3}q_m$ and $\sqrt{4}q_m$, proving the structure at that point being hex-cylinder. Besides, a broad scattering maximum marked by a thick arrow is shifted to $q = 0.72\ \mathrm{nm}^{-1}$, indicating that it corresponds to cylinders rather than spheres as evidenced in the previous work [31].

3.3. TEM observations

Now, we discuss the results on the TEM observations in order to explore the OOT process in detail.

3.3.1. Incubation period

The TEM image given in Fig. 7 shows a transient structure in the incubation period (point (1) in Fig. 3). White broken lines show grain boundaries, so that three grains, G1

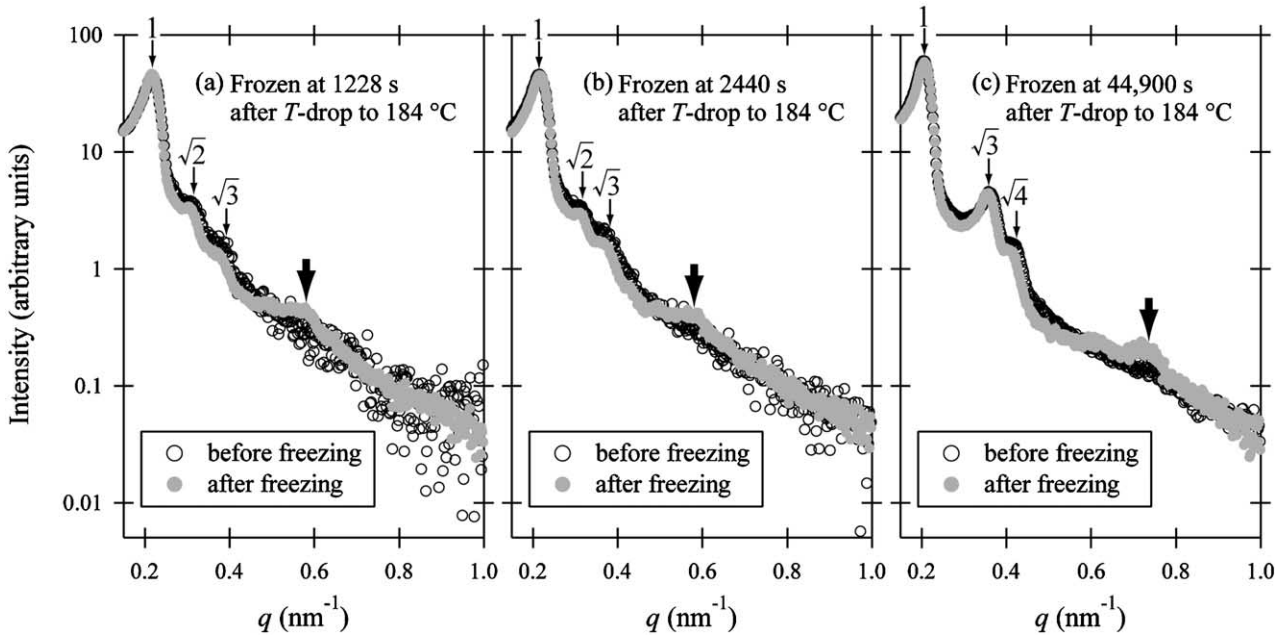

Fig. 6. Comparison of the smeared SAXS profiles measured for the specimens before (black open circles) and after (gray filled circles) freezing at (a) 1228 s, (b) 2440 s and (c) 44,900 s after *T*-drop to 184 °C.

to G3, can be seen in this image. Round bright PS microdomains with a long-range order can be clearly seen in two grains G1 and G2 out of the three. They are packed in a square lattice, which can be clearly seen especially in the inset, which highlights the microdomain structure at the position enclosed by a white square. Considering this image together with the SAXS profiles in Fig. 2 and 6(a), we can conclude that the image reflects (100) plane of bcc-sphere.

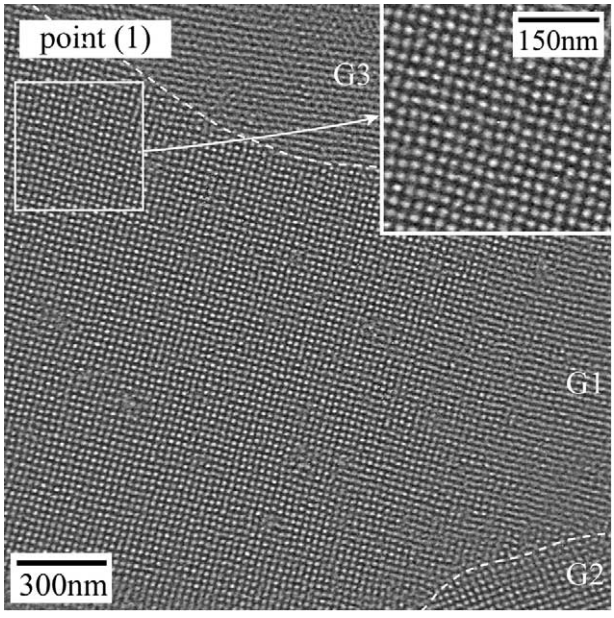

Fig. 7. Transmission electron microscope image for the SIS triblock copolymer frozen at 1228 s (point (1) in Fig. 3). The white broken line traces grain boundaries, and divides into the three grains, G1, G2 and G3. The inset enlarges the region encompassed by the white square.

The microdomain structure in the other grain, G3, is not clear, which is considered to be due to an overlap of bcc-sphere grains along the thickness direction of the ultrathin section, and electron beams propagate along off-symmetry axes with respect to a bcc lattice. Therefore, it is confirmed that the system in the incubation period stays at a super-cooled bcc-sphere state.

3.3.2. *OOT process*

The TEM images given in Fig. 8 show the transient structures at the time just after the OOT started (point (2) in Fig. 3). Fig. 8(a-1) and (b-1) show the different sites of the same specimen, both presenting an ellipsoidal grain with striped microdomains. In order to highlight those grains, a white solid line is drawn on the same images and displayed, respectively, in Fig. 8(a-2) and (b-2). These grains are designated as G′1 and G′3. Further, we note that these grains are enclosed in larger grains designated, respectively, as G′2 and G′4 with more or less round boundaries. The white solid line indicates the grain boundary, which distinguishes the grain with striped microdomains from that with spherical microdomains, while the broken white lines indicate the grain boundary between the gains with bcc-sphere. It is easily found that the white solid line and the white broken line overlap in part in both images ((a-1) and (b-1) or (a-2) and (b-2)). This means that the grain composed of striped microdomains, G′1 and G′3, appears in contact with the grain boundary of G′2 and G′4, respectively. The striped microdomains are considered to be hex-cylinder, judging from the shape of the microdomains and their location in the system. The grains in which the microdomain structures are

not clear also exist in this system, which is due to the same reason as that given in Fig. 7.

3.3.3. Nucleation process of hex-cylinder

It is confirmed even by the TEM observation that hex-cylinder is formed in the matrix of bcc-sphere via the nucleation and growth. Grains, G′1 and G′3, composed of hex-cylinder are invariably generated along a grain boundary of G′2 and G′4 composed of bcc-spheres, respectively. Therefore, it appears to be very likely that defects of bcc-sphere at the vicinity of grain boundaries act as nucleating sites.

There are at least two interpretations for the results concerning relation between the two grains, G′1 and G′2 in Fig. 8(a-2), and G′3 and G′4 in Fig. 8(b-2): (i) The grains of G′1 and G′3 were nucleated inside the grains G′2 and G′4, respectively, and their growth was ceased when the growth front reaches the grain boundaries of G′2 and G′4, respectively; (ii) The grains of G′1 and G′3 were nucleated in the boundaries of the grains G′2 and G′4, respectively, and their growth toward interior of G′2 and G′4, respectively, were frozen by the quench below T_g for the observation of TEM as discussed in Section 2. Close

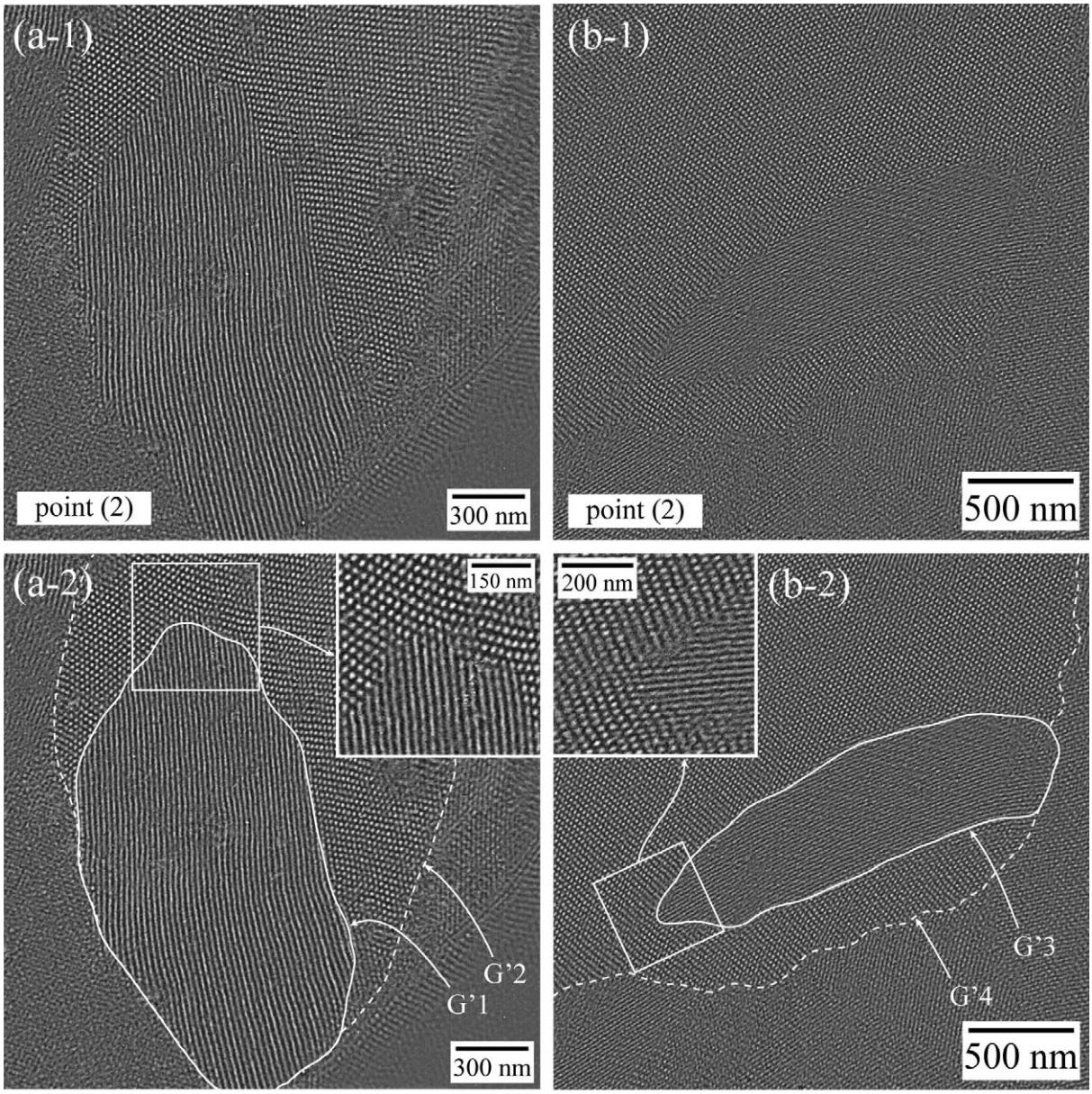

Fig. 8. Transmission electron microscope images for the SIS triblock copolymer frozen at 2440 s (point (2) in Fig. 3). (a-1) and (b-1) show the different sites of the same specimen. (a-2) and (b-2) show just the same images as (a-1) and (b-1), respectively. In (a-2) and (b-2), the white solid lines and the white broken lines encompass the hex-cylinder phase, G′1 or G′3, and the bcc-sphere grain, G′2 or G′4, in which the microdomains can be clearly seen, respectively. The insets in (a-2) and (b-2) enlarge the regions encompassed by the white squares and highlight the grain boundaries between the hex-cylinder phase and the bcc-sphere phase.

observations of many TEM images never showed the images in which the grains of G′1 and G′3 existed inside the grains of G′2 and G′4 without any contacts at their grain boundaries. Therefore, the latter case (ii) seems to be more likely than the former one (i).

The shape of hex-cylinder grains nucleated in bcc-sphere is ellipsoidal. The growth of the grain parallel to cylinder axis seems to be faster than that perpendicular to it. This anisotropic growth is quite different from that observed in ordering of hex-cylinder from disordered sphere reported earlier by Sakamoto and Hashimoto [30]. In the latter case, growth rate was found to be slower along the cylinder axis than perpendicular to the axis, giving rise to the oblate ellipsoidal grains with the cylinder axis being parallel to the axis of revolution.

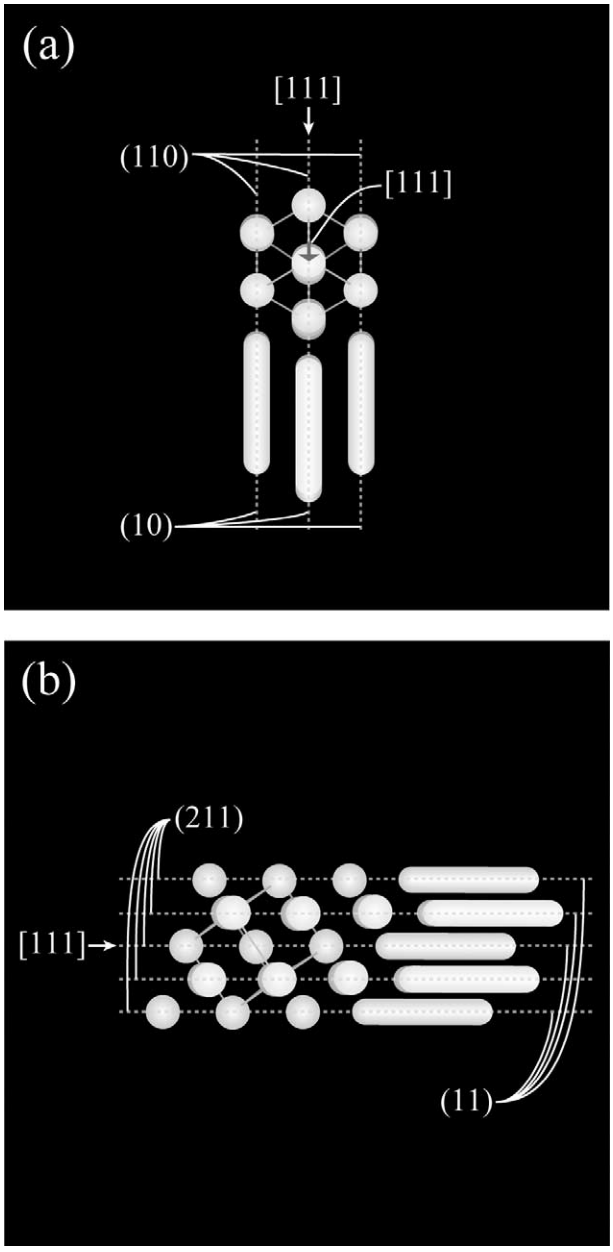

Fig. 9. Schematic illustrations showing the orientation of the microdomains at the vicinity of grain boundaries between hex-cylinder and bcc-sphere. (a) and (b) illustrate the inset of Fig. 8(a-2) and (b-2), respectively. White dotted lines indicate not only the direction of both cylindrical axes and the [111] direction in a bcc lattice but also the symmetry plane perpendicular to the plane of the paper, and white solid lines represent a unit cell of a bcc lattice.

3.3.4. Grain boundary between bcc-sphere and hex-cylinder

The insets in Fig. 8(a-2) and (b-2) highlight the boundary between hex-cylinder and bcc-sphere at the position enclosed by a white square. Now, we would like to define the orientation of the microdomains at the vicinity of the grain boundaries. The spacing of the cylindrical microdomains in the inset of Fig. 8(a-2) is ca. 28 nm. It almost corresponds to D_{10}, obtained by SAXS and shown in Fig. 3(c). Therefore, it can be interpreted as (10) planes in a hexagonal lattice perpendicular to the plane of the paper with its reciprocal lattice vector nearly parallel to the horizontal direction of this figure. Moreover, the spherical microdomains are packed hexagonally in this TEM image. By taking into consideration of the fact that one of four [111] directions in a bcc lattice corresponds to the direction of cylindrical axes on the OOT process, the orientation of the bcc-sphere in the inset of Fig. 8(a-2) can be illustrated as in Fig. 9(a): The cylindrical axes are parallel to one of the [111] axes in a bcc lattice, which points along the vertical direction of the figure, as represented by white dotted lines. White solid lines represent a unit cell of a bcc lattice. Bcc-sphere is viewed along one of the [111] directions, which is perpendicular to the plane of the paper and (110) planes in a bcc lattice are also perpendicular to the plane of the paper. On the other hand, the spacing of the cylindrical microdomains in the inset of Fig. 8(b-2) is ca. 16 nm. It almost corresponds to $D_{10}/\sqrt{3}$, so that (11) planes in a hexagonal lattice are considered to be perpendicular to the plane of the paper with the reciprocal lattice vector approximately parallel to the vertical direction of the figure. The orientation of bcc-sphere in the inset of Fig. 8(b-2) can be illustrated as in Fig. 9(b). White dotted lines and white solid lines are drawn to represent the direction of the cylindrical axes and one of the four [111] directions in a bcc lattice, and a unit cell of a bcc lattice, respectively. A (211) plane in a bcc lattice is also found to be perpendicular to the plane of the paper.

3.3.5. Final stage

As described earlier in conjunction with the SAXS results, D_{110} is needed to be equal to D_{10} when bcc-sphere is transformed to hex-cylinder. As seen in the inset of Fig. 8(a-2), D_{10} looks equal to D_{110} of ca. 28 nm at the vicinity of the grain boundary. D_{10} reaches to ca. 30 nm at the equilibrium state of hex-cylinder according to Fig. 3(c), so that hex-cylinder emerged right after the OOT from bcc-sphere could be still metastable state. The about 2 nm difference between D_{10} right after the OOT and that at the equilibrium state must cause distortion or an excess energy in the newly

nucleated grains composed of hex-cylinder. Therefore, the reason why the three parameters in Fig. 3 changes gradually in period IV even after whole space of the system is filled with hex-cylinder may be attributed to a phenomenon that the strain or excess energy developed during the OOT process has to be released to reach the equilibrium state of hex-cylinder.

Fig. 10 shows the TEM image for the specimen frozen at the time when the OOT is almost completed (point (3) in Fig. 3). White broken lines show grain boundaries. Striped microdomains with long-range order can be seen in the grain, G″1. The spacing of these striped microdomains is ca. 30 nm, corresponding to D_{cyl} according to Fig. 3(c). Therefore, we can conclude that the morphology of the microdomains is hex-cylinder and (10) planes in a hexagonal lattice are perpendicular to the plane of the paper. The microdomain structures in the grains, G″2 and G″3, are not clear. It is probably because the orientation of hex-cylinder in those grains is off symmetry planes. In any case, we found that hex-cylinder fills the whole sample space at this time.

The TEM results described above are consistent with the SAXS results. Especially, in period II and III, the coexistence of bcc-sphere and hex-cylinder can be also observed in the TEM image. Therefore, it is really confirmed that the OOT from bcc-sphere to hex-cylinder proceeds via the nucleation and growth process as predicted by theoretical studies [25].

3.4. Quench-depth dependence of the OOT processes from bcc-sphere to hex-cylinder

So far, we have presented the OOT process only at the given ΔT (=4 K). We shall now discuss the quench-depth dependence of the OOT processes. Fig. 11 shows the time evolutions of (a) I_m, (b) σ_q^2, and (c) D at ΔT=4, 6, 8, and 10 K. The trend for the time evolution of each parameter is found to be almost the same for the four quenches. The deeper the quench depth is, the faster the OOT proceeds. Comparing these three figures, we note that the best way of tracing the OOT process is to investigate the time evolution of D. The reason is as follows: As for I_m, it is difficult to discern the time when the OOT starts, because I_m still indicates a constant value even after the incubation period as shown earlier for ΔT=4 K (Fig. 3(a)). In addition, there are disparities of I_m by about 30% at different values of ΔT in the late stage of period IV, due primarily to temperature dependence electron density difference between the two microphases, as will be clarified later in conjunction with Fig. 13. As for σ_q^2, the data in the incubation time is somewhat fluctuating. Therefore, it is difficult to discern the time when the OOT starts, only from the time evolution of σ_q^2. Additionally, the maximum value of σ_q^2 in each time evolution is different, because a number of generated grains composed of hex-cylinder in the matrix of the bcc-sphere phase depends on ΔT. It becomes large when many small grains exist in the system. Thus, it is not suitable to compare the OOT processes by the time evolutions of I_m and σ_q^2. In contrast, D in the incubation period is about 28 nm for the time evolutions at all ΔTs, and then it starts to increase when the OOT starts. As described in Section 3.1.2, the first-order peak position of hex-cylinder locates at a smaller q_m than that of bcc-sphere. Therefore, the first-order peak is shifted to smaller q as the grains of hex-cylinder grow at the expense of the bcc-sphere phase, so that D increases as shown in Fig. 11(c). Finally, D approaches ca. 30 nm gradually. Consequently, the time evolution of D is a quite useful structural parameter for exploring the OOT process.

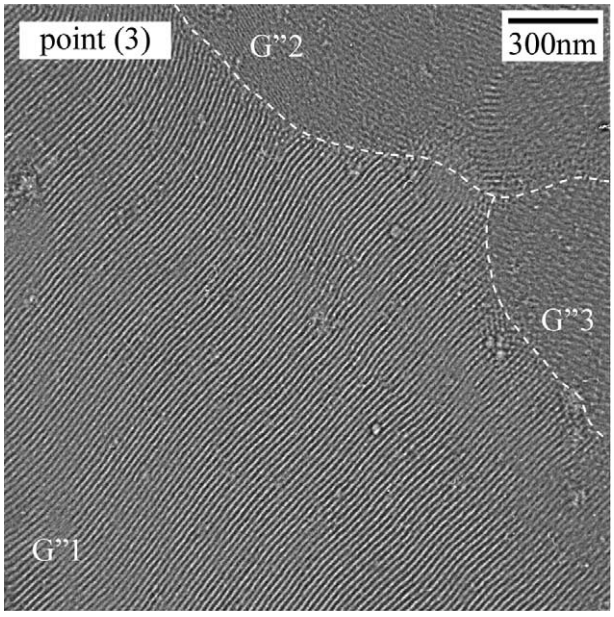

Fig. 10. Transmission electron microscope images for the SIS triblick copolymer frozen at 44,900 s (point (3) in Fig. 3). The white broken line traces grain boundaries and divides into the three grains, G″1, G″2 and G″3.

Then, the time evolutions of D in Fig. 11(c) are replotted as a function of the reduced time, t/t_i, in Fig. 12(a), where t_i is the incubation time for the OOT process defined as the time (shown by the arrow in Figs. 11(c) and 12(c)) when D vs log t starts deviate from the linear relationship as shown by the gray line in Fig. 12(c), to qualitatively compare the OOT processes at the four quenches. Moreover, t_i is plotted as a function of ε and ΔT in Fig. 12(b). It is found from Fig. 12(a) that all the curves fall onto a master curve. This fact suggests that the mechanism of the OOT at $178 < T_{cyl} < 184$ °C is essentially identical: All the OOT processes proceed via the nucleation and growth process; The rate of the OOT is slowed down accordingly with the prolonged t_i. The latter is confirmed by the plot of $t_{1/2}$ vs ε, also shown in Fig. 12(b). Here, $t_{1/2}$ is defined in Fig. 12(c) as follows: D changes from D_i to D_f during the OOT process (i.e. from the point A to C in Fig. 3), where D_i and D_f are the D values at t_i and t_f, respectively, and definition of t_f is the same as that of point C in Fig. 3. Thus, $t_{1/2}$ is defined as $t_m - t_i$, where t_m is the time when D reaches D_m defined by $(D_i + D_f)/2$. The value, $t_{1/2}^{-1}$ is related to the rate of the OOT. Fig. 12(b) reveals that there is linearity between log t_i and ε and between log $t_{1/2}$

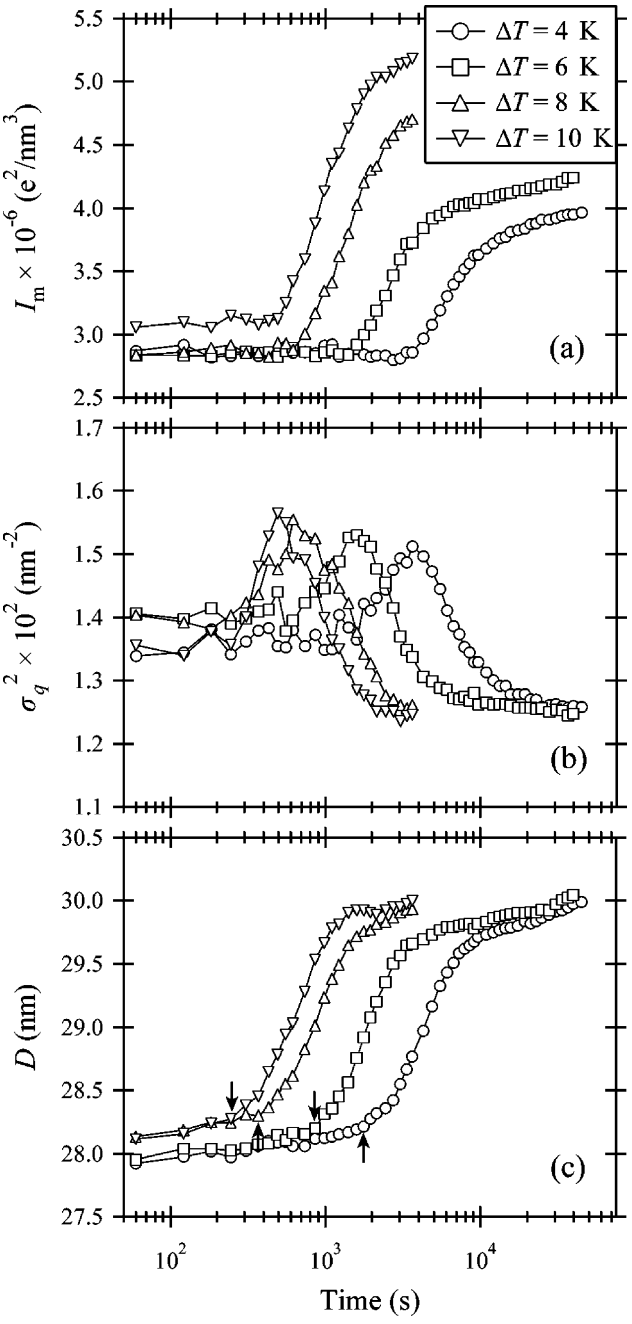

Fig. 11. Time evolutions of (a) the peak intensity, I_m, (b) the square of the half-width at half maximum, σ_q^2, (c) the Bragg spacing, D, of the desmeared SAXS profile for the SIS triblock copolymer after T-drop from 195 to 178, 180, 182, and 184 °C. The arrows indicate the onset of the OOT.

and ε as given by:

$$\log t_i = 3.82 - 67.8\varepsilon \quad (1)$$

$$\log t_{1/2} = 3.93 - 69.0\varepsilon \quad (2)$$

The fact that $\log t_i$ vs ε and $\log t_{1/2}$ vs ε show essentially parallel behavior indicates that the system has only a single time scale, confirming the latter statement described above that a change of t_i with ΔT causes a related change in the rate

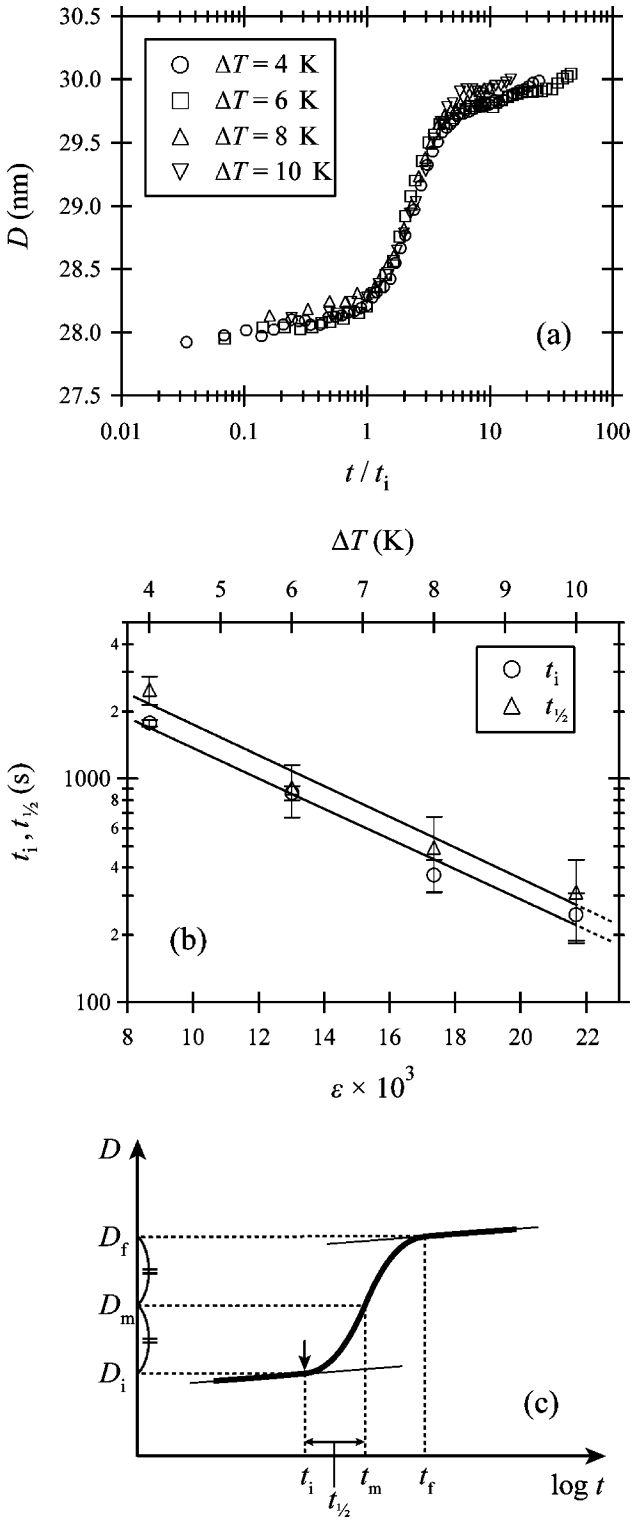

Fig. 12. (a) Bragg spacing, D, plotted as the reduced time, t/t_i, where t_i is the incubation time. (b) The incubation time, t_i, and the half time, $t_{1/2}$, for the OOT process defined in part (c), plotted as the thermodynamic driving force, ε, and ΔT. (c) Definitions of an incubation time t_i and a half time, $t_{1/2}$, in the time evolution of Bragg spacing, D.

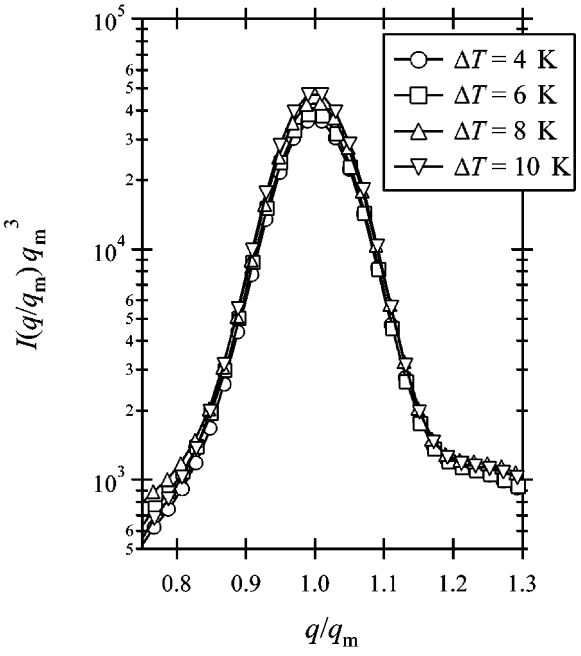

Fig. 13. Temperature dependence of the scaled structure factors in the late stage of the OOT process where the hex-cylinder phase is volume filling. The scaled structure factors are shown to be essentially universal with ΔT.

of the OOT process. It is also clear that ΔT affects only the rate of the OOT process but not the mechanism at least in the range of ΔT studied.

However, if ΔT is further increased, $\Delta T \gg 10$ K, it is anticipated that the OOT would proceed by another mechanism, i.e. spinodal decomposition. The incubation time could hardly been observed under this condition. Indeed, it is a very interesting topic to investigate the OOT process induced by $\Delta T \gg 10$ K, which will be discussed in the other paper [46].

Finally, we would like to note that we obtained the universal scaled structure factor with time at each ΔT for the late stage of the OOT processes in the volume-filled hex-cylinder phase as shown in Fig. 4(b) at $\Delta T = 4$ K. The scaled structure factors obtained at the different ΔTs are also independent of ΔT, except for a small difference in the absolute intensity level by about 30% as shown in Fig. 13. The larger the value ΔT is, the larger the intensity is. The main part of the structure factors as different ΔTs can be superposed into one curves by the vertical shift in the semi logarithmic plot. The difference in the intensity levels for different ΔTs may be due to a small ΔT dependence of electron density difference between the PS cylinder and PI matrix, which, in turn, may be due to ΔT dependence of difference in thermal expansion coefficients between the cylinder and matrix. According to the literature on temperature dependence of specific volume for PS and PI [47], the electron density difference between PS domains and PI domains at 178 °C ($\Delta T = 10$ K) can be larger than that at 184 °C ($\Delta T = 4$ K) by ca. 7% at most within the accuracy of the reported results. Thus, the small difference in the absolute intensity level (by ~30%) may be explained in terms of thermal expansion within the experimental errors.

4. Concluding remarks

We have succeeded in the *real-time* observation of the OOT process from bcc-sphere to hex-cylinder for the SIS triblock copolymer by means of the time-resolved SAXS measurements as well as by means of the TEM observations of the samples frozen during the OOT process. As a consequence, we have elucidated the mechanism and kinetics of the OOT as follows: After T-drop, the system stays at a metastable or supercooled bcc-sphere state for a certain incubation period. The incubation time depends on quench depth, ΔT. Grains composed of hex-cylinder are nucleated at grain boundaries of the poly-grain state of bcc-sphere. Hex-cylinder grows along one of the [111] directions of bcc-sphere. When bcc-sphere is transformed into hex-cylinder, the spacing of (110) planes in bcc-sphere is required to be increased so as to match that of (10) planes in hex-cylinder. However, it is found in this study that there is about 2 nm difference between them. This mismatch is important for determining the rate of the OOT. The grains of hex-cylinder go on growing, and finally hex-cylinder fills the whole space. Even if hex-cylinder is formed, the strain should still remain in the as-formed hex-cylinder, due to the difference of the Bragg spacing between bcc-sphere and equilibrium hex-cylinder. The strain continues to be released in order to reach an equilibrium state of hex-cylinder at T_{cyl}. All the OOT processes in this study can be expressed by a single time scale, t_i or $t_{1/2}$, which depends on ΔT, so that the OOT in $\Delta T \leq 11$ proceeds via the nucleation and growth process, reflecting the first-order phase transition. It is found that the incubation time, t_i, and the rate of the OOT process, $t_{1/2}^{-1}$, are closely interrelated, both of which have almost the same ΔT dependence.

Acknowledgements

The authors gratefully acknowledge Prof. C. D. Han for providing the interesting block copolymer sample. T. H. gratefully acknowledges financial support by 21st Century COE Program for a United Approach to New Materials Science.

References

[1] Kim JK, Lee HH, Ree M, Lee K-B, Park Y. Macromol Chem Phys 1998;199:641–53.
[2] Sakamoto N, Hashimoto T, Han CD, Kim D, Vaidya NY. Macromolecules 1997;30:1621–32.
[3] Sakurai S, Kawada H, Hashimoto T, Fetters LJ. Macromolecules 1993;26:5796–802.
[4] Sakurai S, Hashimoto T, Fetters LJ. Macromolecules 1996;29:740–7.

[5] Ryu CY, Lee MS, Hajduk DA, Lodge TP. J Polym Sci, Polym Phys Ed 1997;35:2811–23.
[6] Ryu CY, Lodge TP. Macromolecules 1999;32:7190–201.
[7] Kimishima K, Koga T, Hashimoto T. Macromolecules 2000;33: 968–77.
[8] Matsen MW, Bates FS. Macromolecules 1996;29:1091–8.
[9] Matsen MW, Bates FS. J Chem Phys 1997;106:2436–48.
[10] Förster S, Khandpur AK, Zhao J, Bates FS, Hamley IW, Ryan AJ, et al. Macromolecules 1994;27:6922–35.
[11] Khandpur AK, Förster S, Bates FS, Hamley IW, Ryan AJ, Bras W, et al. Macromolecules 1995;28:8796–806.
[12] Bates FS, Fredrickson GH. In: Legge NR, Holden GR, Schroeder HE, editors. Thermoplast elastomers. 2nd ed. Vienna: Hanser; 1996. p. 335 [chapter 12].
[13] Helfand E, Wasseman ZR. In: Goodman I, editor. Developments in block copolymers, vol. 1. London: Applied Science; 1982. p. 99 [chapter 4].
[14] Hashimoto T, Shibayama M, Fujimura M, Kawai H. In: Meier DJ, editor. Block copolymers, science and technology. London: Harwood Academic Publishers; 1983. p. 63.
[15] Leibler L. Macromolecules 1980;13:1602–17.
[16] Fredrickson GH, Helfand E. J Chem Phys 1987;87:697–705.
[17] Vavasour JD, Whitmore MD. Macromolecules 1992;25:5477–86.
[18] Qi S, Wang Z-G. Phys Rev Lett 1996;76:1679–82.
[19] Qi S, Wang Z-G. Phys Rev E 1997;55:1682–97.
[20] Qi S, Wang Z-G. Polymer 1998;39:4639–48.
[21] Laradji M, Shi A-C, Desai RC, Noolandi J. Phys Rev Lett 1997;78: 2577–80.
[22] Laradji M, Shi A-C, Noolandi J, Desai RC. Macromolecules 1997;30: 3242–55.
[23] Shi A-C, Noolandi J. Polymer 1998;39:4649–54.
[24] Shi A-C. J Phys: Condens Matter 1999;11:10183–97.
[25] Matsen MW. J Chem Phys 2001;114:8165–73.
[26] Koppi KA, Tirrell M, Bates FS, Almdal K, Mortensen K. J Rheol 1994;38:999–1027.
[27] Kim JK, Lee HH, Gu Q-J, Chang T, Jeong YH. Macromolecules 1998; 31:4045–8.
[28] Lee HH, Jeong W-Y, Kim JK, Ihn KJ, Kornfield JA, Wang Z-G, et al. Macromolecules 2002;35:785–94.
[29] Sota N, Saijo K, Hashimoto T, Ito K, Amemiya Y. In preparation.
[30] Sakamoto N, Hashimoto T. Macromolecules 1998;31:8493–502.
[31] Sota N, Sakamoto N, Saijo K, Hashimoto T. Macromolecules 2003; 36:4534–43.
[32] Han CD, Vaidya NY, Kim D, Shin G, Yamaguchi D, Hashimoto T. Macromolecules 2000;33:3767–80.
[33] Vaidya NY, Han CD, Kim D, Sakamoto N, Hashimoto T. Macromolecules 2001;34:222–34.
[34] Fujimura M, Hashimoto H, Kurahashi K, Hashimoto T, Kawai H. Macromolecules 1981;14:1196–202.
[35] Fujimura M, Hashimoto T, Kawai H. Mem Fac Eng, Kyoto Univ 1981;43(2):224.
[36] Hashimoto T, Suehiro S, Shibayama M, Saijo K, Kawai H. Polym J 1981;13:501–16.
[37] Suehiro S, Saijo K, Ohta Y, Hashimoto T, Kawai H. Anal Chim Acta 1986;189:41–56.
[38] Kortleve G, Tuynman CAF, Vonk CG. J Polym Sci, Part A-2: Polym Phys 1972;10:123–31.
[39] Medellin-Rodriguez FJ, Philips PJ, Lin JS. Macromolecules 1996;29: 7491–501.
[40] Hendricks RW. J Appl Crystallogr 1972;5:315–24.
[41] Kato K. J Polym Sci, Part B: Polym Lett 1966;4:35–8.
[42] Ribbe AE, Bodycomb J, Hashimoto T. Macromolecules 1999;32: 3154–6.
[43] Binder K, Stauffer D. Phys Rev Lett 1974;33:1006–9.
[44] Hashimoto T. Phase Transitions 1988;12:47–119.
[45] Hashimoto T. In: Cahn RW, Haasen P, Kramer J, editors. Materials science and technology. Structure and properties of polymers, vol. 12. Weinheim: VCH; 1993. p. 251–300 [chapter 6].
[46] Sota N, Hashimoto T. In preparation.
[47] In: Brandrup J, Immergut EH, Grulki EA, editors. Polymer Handbook. 4th ed. vol 1. Hoboken: Wiley-Interscience; [section V].